Electronic Excitation Response of DNA to High-Energy Proton Radiation in Water

Christopher Shepard[1], Dillon C. Yost,[3] and Yosuke Kanai[1,2,*]

[1]*Department of Chemistry, University of North Carolina at Chapel Hill, Chapel Hill, North Carolina 27514, USA*
[2]*Department of Physics and Astronomy, University of North Carolina at Chapel Hill, Chapel Hill, North Carolina 27514, USA*
[3]*Department of Materials Science and Engineering, Massachusetts Institute of Technology, Cambridge, Massachusetts 02139, USA*

The lack of molecular-level understanding for the electronic excitation response of DNA to charged particle radiation, such as high-energy protons, remains a fundamental scientific bottleneck in advancing proton and other ion beam cancer therapies. In particular, the dependence of different types of DNA damage on high-energy protons represents a significant knowledge void. Here we employ first-principles real-time time-dependent density functional theory simulation, using a massively parallel supercomputer, to unravel the quantum-mechanical details of the energy transfer from high-energy protons to DNA in water. The calculations reveal that protons deposit significantly more energy onto the DNA sugar-phosphate side chains than onto the nucleobases, and greater energy transfer is expected onto the DNA side chains than onto water. As a result of this electronic stopping process, highly energetic holes are generated on the DNA side chains as a source of oxidative damage.

Introduction.—Understanding the radiation-induced response of DNA is pivotal for human health. The electronic excitation induced in DNA by high-energy protons is of great importance to understanding how DNA damage occurs in extreme conditions such as those experienced by astronauts. For instance, as much as 90% of galactic cosmic radiation (GCR) is high-energy protons, and human exposure to GCR is a great concern for space missions, as limited data exist on the bodily effects [1]. The electronic excitation response of DNA to high-energy protons is also the foundation of modern proton beam cancer therapy. Over the past 30 years, proton beam therapy has emerged as a promising alternative to conventional x rays in radiation oncology [2]. Having a spatially localized energy deposition profile, with the so-called Bragg peak being its maximum, the ion beam can more precisely target tumor cells, while minimally affecting surrounding healthy cells [3,4]. In proton beam therapy, the energy deposition profile needs to be developed for individual patients, and the velocity-dependent energy transfer rate from irradiating protons in water plays a central role [5,6]. This quantity, often called linear energy transfer or electronic stopping power, is given per unit distance traveled by irradiating protons. The initial kinetic energy of the protons is on the order of a few hundred MeV. As the protons slow down by transferring their momentum, the stopping power increases greatly near the Bragg peak velocity. In addition to having the ideal energy transfer behavior, many studies indicate that proton beams yield complex clustering lesions with strand breaks, including double-strand breaks, as the direct effect on DNA [7]. These strand lesions, particularly with other lesions nearby, are much more likely to lead to cell death [8]. However, how

the proton beam induces DNA lesions is not understood at the molecular level [9], and details of the energy transfer mechanism from irradiating protons to DNA are needed to help fill this crucial knowledge gap [10]. The ultrafast nature of the excitations and the need for a particle accelerator, like a cyclotron, to generate high-energy protons makes experimental investigation difficult [11]. On the theory side, perturbation theories based on the dielectric function are widely used, and the current state-of-the-art approach builds on developing an accurate energy-loss function for dry DNA and liquid water as the target [12–15]. Modern quantum-mechanical simulation offers an alternative approach for investigating such electronic stopping phenomena on the molecular level [16,17]. Nonequilibrium simulations of electron dynamics have significantly benefited from recent advances in massively parallel computers [18], and unraveling the quantum-mechanical details at the molecular level has impacted various research areas [19,20]. In particular, with the development of time-dependent density functional theory in its explicit real-time propagation form (RT TDDFT), it is now possible to investigate the quantum dynamic response of electrons in systems of great chemical complexity, such as DNA in water, as required here for studying electronic stopping. Using large-scale RT TDDFT simulations [20–22], we show here that high-energy protons transfer significantly more energy to the sugar-phosphate side chains than the nucleobases of DNA, generating highly energetic holes on the side chains as key source of oxidative damage.

Results and discussion.—Figure 1 shows B-DNA (i.e., normal right-handed DNA [23]), solvated in water, with the simulation cell outlined by the black box. The DNA strand
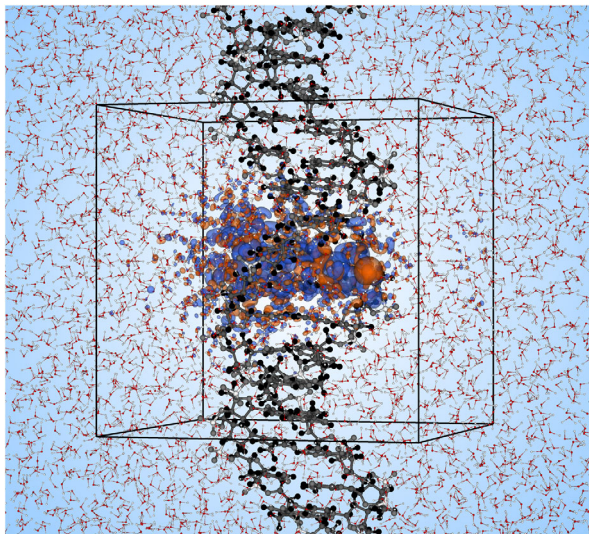
FIG. 1. Simulation cell for solvated DNA. The simulation cell, outlined in black, is shown with periodic boundary conditions for solvated DNA. Blue (orange) isosurfaces represent decreases (increases) in electron density in response to a proton moving through the center of DNA at 0.50 a.u. velocity (6.25 keV).

within the simulation cell comprises one full turn of the double helix. Including the surrounding water molecules, the dynamics of more than 11 500 electrons are explicitly simulated as they respond to an irradiating proton. Additional computational details are discussed in the "Computational Method" section of the Supplemental Material [24]. In our previous work on dry DNA [48], this first-principles approach was used and compared to the widely used semiempirical perturbation theory formalism, based on the dielectric function [12], showing good agreement. We consider two paths for an irradiating proton as shown in Fig. 2(a): the base path directly through the center of the DNA molecule [shown in cyan in Fig. 2(a) herein and

Fig. S1 in Supplemental Material [24]] and the side path along the sugar-phosphate side chain [shown in red in Fig. 2(a) herein and Fig. S1 [24]]. Simulations were performed at six different proton kinetic energies (0.5–6.0 a.u. velocity, or equivalently 6.25–900 keV kinetic energy) for each path, including velocities close to the Bragg peak in dry DNA [48] and liquid water [49]. All atoms, other than the irradiating proton, are fixed in place to study the electronic stopping phenomenon here, and the timescale of each simulation (0.27–3.38 fs, depending on proton velocity) is too short for any significant nuclear motion [50]. The energy transfer rate, referred to as electronic stopping power, can be obtained as a function of the proton velocity for each individual path [51]. It is convenient to express the stopping power in terms of the work done on the nonequilibrium system of electrons by a single "projectile" proton, and the total electronic energy change of the system can be used in practical computation of the stopping power (see Supplemental Material for details [24]) [20]. Comparison of the solvated DNA stopping power curves [Fig. 2(b), solid lines] reveals that the stopping power magnitude for the side path is more than 3 times larger than that for the base path at the peak, and at least twice as large at all velocities. This difference increasingly diminishes with higher proton velocities. While the Bragg peak positions for both paths remain similar to that of liquid water [49] [Fig. 2(b), black line], the stopping power magnitude for the side path is 40% larger at the Bragg peak. This is of particular importance as the electronic stopping power for liquid water is generally used for calibrating proton beam in radiation oncology [52]. We also note that at the higher velocities of 4.00 and 6.00 a.u., the stopping power magnitude for the side path is nearly identical to that of liquid water. Compared to the case of dry DNA [48], the side path also shows much larger electronic stopping power for solvated DNA (see Fig. S3 in Ref. [24]).
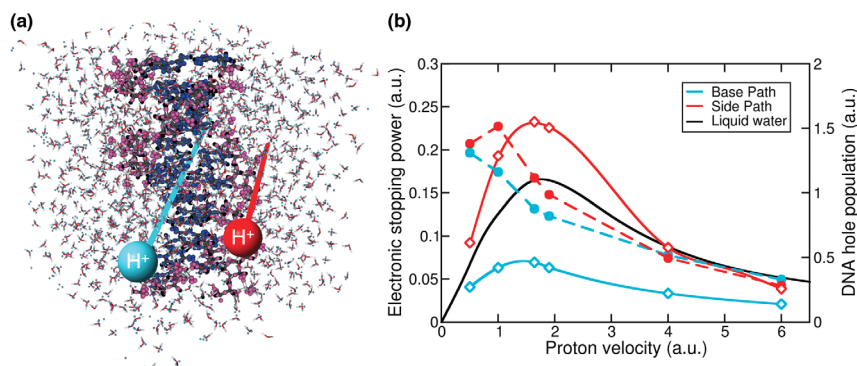

FIG. 2. Electronic stopping power for protons in solvated DNA. (a) Solvated DNA structure, with ground state MLWFs shown as light blue spheres (water), dark blue spheres (nucleobases), and magenta spheres (sugar-phosphate side chain). The base path is denoted by the cyan line and the side path is denoted by the red line. (b) Electronic stopping power for the base and side paths is shown with solid lines, calculated as the average instantaneous stopping power over the DNA-interaction region (see Supplemental Material for details). The electronic stopping power of liquid water is shown for reference with a solid black line [49]. DNA hole populations, taken at the end of each path, are shown with dashed lines.

Negative charges, specifically lone-pair electrons on phosphate groups on the DNA side chains, were found to be largely responsible for this difference (see Supplemental Material for details [24]). In order to gain molecular-level insights in this complex system, we employ the time-dependent maximally localized Wannier function (TD MLWF) gauge [53,54]. TD MLWFs are spatially localized on different chemical moieties, creating a chemically intuitive picture of the DNA-water electronic system. Geometric centers of the TD MLWFs, commonly referred to as Wannier centers, are shown in Fig. 2(a). The TD MLWFs can be grouped into different chemical subgroups, and the electronic response of DNA can be separated from that of the solvating water molecules. The response is further studied in terms of DNA chemical moieties, nucleobases, and sugar-phosphate side chains, by analyzing changes to the spatial spread (Wannier center variance) and Wannier center displacement of individual TD MLWFs. Figure 3 shows the Wannier center displacements [Fig. 3(a)] and spread changes [Fig. 3(b)] for the two paths at the proton velocity of 1.64 a.u. (67.19 keV), close to the Bragg peak. For both paths, greater than 80% of the Wannier center displacements are within 10 a.u. of the proton path, and more than 90% of the spread changes are
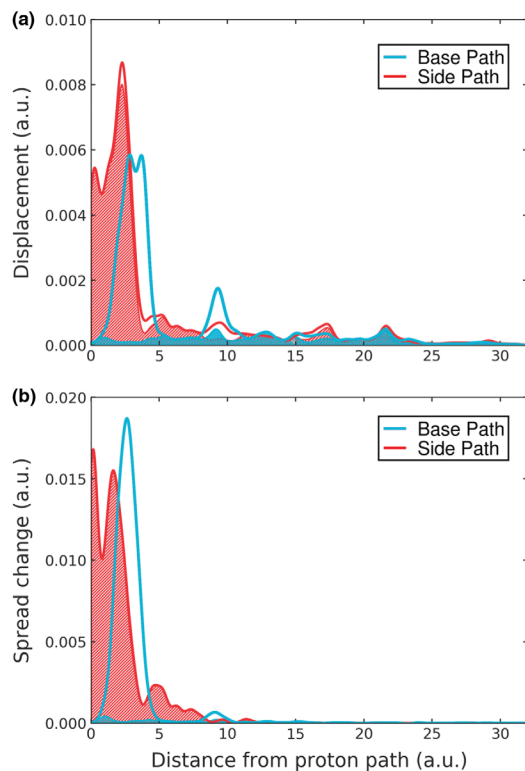

FIG. 3. Displacement and spread change of DNA TD MLWFs for the proton velocity of 1.64 a.u. (a) Displacement (measure of electronic movement) of the DNA TD MLWF centers. (b) Spread change (measure of electronic delocalization) of DNA TD MLWF centers. Hatched regions correspond to contributions from the phosphate side chain.

within 5 a.u. of the proton path; the electronic excitation response is highly localized near the path of the irradiating proton. In Fig. 3, the hatched areas indicate contributions from the sugar-phosphate side chain. The response for the side path is almost entirely from the phosphate side chain, greater than 87% of the displacements and more than 98% of the spread changes, while the base path shows minimal contribution from the phosphate side chain, with over 75% of the displacements and more than 90% of the spread change from nucleobases. These key excitation features are also observed at higher and lower velocities (see Figs. S6 and S7 in Supplemental Material [24]). Our simulations show that the sugar-phosphate side chain molecules absorb much more energy than nucleobases in the proton beam.

Electronic stopping power is often thought to be directly proportional to electronic excitations, or more specifically, the number density (i.e., population) of holes (or excited electrons) generated under ionizing radiation [55]. Figure 2(b) also shows the formation of holes on DNA as a function of the irradiating proton velocity (dashed lines). The DNA hole populations were found to reach a constant value by the end of each simulation trajectory, and charge transfer from DNA to the irradiating proton does not contribute to the hole population (see Supplemental Material for details [24]). While the stopping power is considerably different between the two paths, the hole population is only slightly larger for the side path. For the 1.00 a.u. proton velocity, where the largest difference in DNA hole population is observed, 1.3 times as many holes are generated for the side path relative to the base path. However, the stopping power is more than 3 times greater for the side path at the same velocity, relative to the base path. Therefore, the differences in electronic stopping power cannot be explained simply by the number density of holes formed on DNA. The stopping power also depends on the energetics of the generated holes. To quantify the energetics, we project the DNA-localized TD MLWFs onto the energy eigenstates. Figure 4 shows the hole population on DNA as a function of energy for the base path [Fig. 4(a)] and the side path [Fig. 4(b)]. The electronic density of states is also shown as a reference (dashed line). A significant number of holes are formed in the deeper lying states for the side path, and essentially no holes are formed within approximately 2 eV of the highest occupied molecular orbital (HOMO), which is aligned at 0 eV in Fig. 4. The HOMO in DNA largely comprises nucleobase electronic states, and the base path shows a sharp peak close to HOMO, which is responsible for 10%–15% of the holes generated on DNA, depending on the irradiating proton velocity. The deeper-lying DNA states, at around −20 eV, largely derive from the DNA sugar-phosphate side chains. For the side path, as much as 8% of the total DNA holes are generated between −20 and −25 eV. At the same time, holes generated in this energy range represent only 2% or less of the total hole population for the base path,
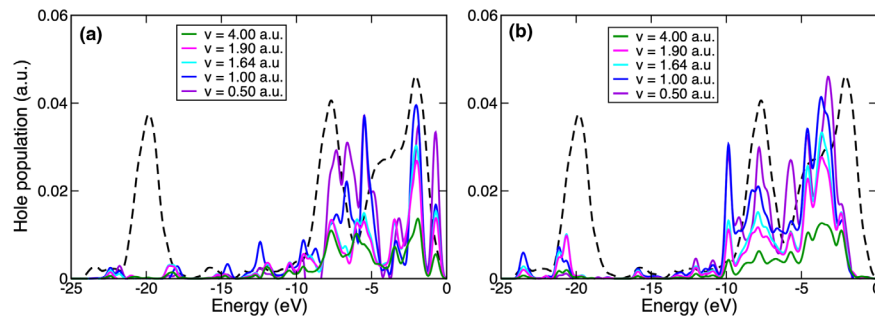
FIG. 4. DNA hole populations as a function of energy for the base (a) and side (b) paths. DNA TD MLWFs are projected onto the eigenstates of the system at equilibrium to calculate the energies at which holes are generated in DNA at the end of simulations. For reference, the density of states is shown with a dashed line. Gaussian broadening of 0.25 eV was used for all hole energy distributions. HOMO is aligned to be at 0 eV. Nearly identical energetics were observed at the end of the DNA-interaction region (see Figs. S10 and S11 in Supplemental Material [24]).

depending on the proton velocity. This characteristic difference in hole energetics is largely responsible for the significant difference in the stopping power for these two paths, and more extensive DNA phosphate side chain damage can be expected than DNA nucleobase damage, under proton irradiation. Additionally, at velocities away from the Bragg peak (e.g., 4.00 and 0.50 a.u., above and below the Bragg peak, respectively), the hole generation in the deeper-lying regions (corresponding to the sugar-phosphate side chains) becomes quite small, as seen in Fig. 4. Thus, significant strand damage to DNA can be expected only for proton velocities close to the Bragg peak.

Conclusion.—The electronic excitation response of DNA to high-energy protons in water was investigated. Quantum-mechanical simulations revealed intricate molecular-level details of the energy transfer process from the high-energy protons to DNA in water. With proton irradiation, significantly more energy was deposited onto the sugar-phosphate side chains rather than onto the nucleobases. The enhanced energy transfer to the DNA strands derives from the generation of highly energetic holes on the side chains. These highly energetic holes are a key source of oxidative damage, and their formation on the side chains is likely the source of DNA strand damage. The first-principles simulation results presented here fill a key knowledge void in understanding detailed mechanisms for extensive DNA strand break lesions observed with a proton beam. In the context of proton beam cancer therapy, the present Letter will add to the growing knowledge base for building increasingly more sophisticated multiscale modeling in medical physics [15,56,57].

*Corresponding author.
 ykanai@unc.edu

[1] J. C. Chancellor, R. S. Blue, K. A. Cengel, S. M. Auñón-Chancellor, K. H. Rubins, H. G. Katzgraber, and A. R. Kennedy, Limitations in predicting the space radiation health risk for exploration astronauts, npj Microgravity **4**, 8 (2018).

[2] M. Durante and J. S. Loeffler, Charged particles in radiation oncology, Nat. Rev. Clin. Oncol. **7**, 1 (2010).

[3] B. Patyal, Dosimetry aspects of proton therapy, Technol. Cancer Res. Treat. **6**, 4 Suppl (2007).

[4] W. P. Levin, H. Kooy, J. S. Loeffler, and T. F. DeLaney, Proton beam therapy, Br. J. Cancer **93**, 8 (2005).

[5] H. Paganetti, Relative biological effectiveness (RBE) values for proton beam therapy. Variations as a function of biological endpoint, dose, and linear energy transfer, Phys. Med. Biol. **59**, 22 (2014).

[6] H. Paganetti, A. Niemierko, M. Ancukiewicz, L. E. Gerweck, M. Goitein, J. S. Loeffler, and H. D. Suit, Relative biological effectiveness (RBE) values for proton beam therapy, Int. J. Radiat. Oncol. Biol. Phys. **53**, 2 (2002).

[7] S. Girdhani, R. Sachs, and L. Hlatky, Biological effects of proton radiation: What we know and don't know, Radiat. Res. **179**, 3 (2013).

[8] E. T. Vitti and J. L. Parsons, The radiobiological effects of proton beam therapy: Impact on DNA damage and repair, Cancers (Basel) **11**, 7 (2019).

[9] P. Chaudhary, T. I. Marshall, F. J. Currell, A. Kacperek, G. Schettino, and K. M. Prise, Variations in the processing of DNA double-strand breaks along 60-MeV therapeutic proton beams, Int. J. Radiat. Oncol. Biol. Phys. **95**, 86 (2016).

[10] J. S. Loeffler and M. Durante, Charged particle therapy—Optimization, challenges and future directions, Nat. Rev. Clin. Oncol. **10**, 7 (2013).

[11] J. M. Schippers, A. Lomax, A. Garonna, and K. Parodi, Can technological improvements reduce the cost of proton radiation therapy?, Semin. Radiat. Oncol. **28**, 150 (2018).

[12] I. Abril, R. Garcia-Molina, C. D. Denton, I. Kyriakou, and D. Emfietzoglou, Energy loss of hydrogen- and helium-ion beams in DNA: Calculations based on a realistic energy-loss function of the target, Radiat. Res. **175**, 2 (2010).

[13] H. Nikjoo, D. Emfietzoglou, T. Liamsuwan, R. Taleei, D. Liljequist, and S. Uehara, Radiation track, DNA damage and response—A review, Rep. Prog. Phys. **79**, 11 (2016).

[14] D. Emfietzoglou, G. Papamichael, and H. Nikjoo, Monte Carlo electron track structure calculations in liquid water using a new model dielectric response function, Radiat. Res. **188**, 3 (2017).

[15] I. Kyriakou, D. Sakata, H. N. Tran, Y. Perrot, W.-G. Shin, N. Lampe, S. Zein, M. C. Bordage, S. Guatelli, C. Villagrasa, D. Emfietzoglou, and S. Incerti, Review of the Geant4-DNA simulation toolkit for radiobiological applications at the cellular and DNA level, Cancers (Basel) **14**, 1 (2022).

[16] D. C. Yost, Y. Yao, and Y. Kanai, First-principles modeling of electronic stopping in complex matter under ion irradiation, J. Phys. Chem. Lett. **11**, 229 (2020).

[17] A. Alvarez-Ibarra, A. Parise, K. Hasnaoui, and A. de la Lande, The physical stage of radiolysis of solvated DNA by high-energy-transfer particles: Insights from new first principles simulations, Phys. Chem. Chem. Phys. **22**, 7747 (2020).

[18] T. W. Keal, A. M. Elena, A. A. Sokol, K. Stoneham, M. I. J. Probert, C. S. Cucinotta, D. J. Willock, A. J. Logsdail, A. Zen, P. J. Hasnip, I. J. Bush, M. Watkins, D. Alfè, C. K. Skylaris, B. F. E. Curchod, Q. Cai, and S. M. Woodley, Materials and molecular modeling at the exascale, Comput. Sci. Eng. **24**, 36 (2022).

[19] X. Li, N. Govind, C. Isborn, A. E. DePrince, and K. Lopata, Real-time time-dependent electronic structure theory, Chem. Rev. **120**, 9951 (2020).

[20] A. Schleife, E. W. Draeger, V. M. Anisimov, A. A. Correa, and Y. Kanai, Quantum dynamics simulation of electrons in materials on high-performance computers, Comput. Sci. Eng. **16**, 5 (2014).

[21] C. Shepard, R. Zhou, D. C. Yost, Y. Yao, and Y. Kanai, Simulating electronic excitation and dynamics with real-time propagation approach to TDDFT within plane-wave pseudopotential formulation, J. Chem. Phys. **155**, 10 (2021).

[22] E. W. Draeger, X. Andrade, J. A. Gunnels, A. Bhatele, A. Schleife, and A. A. Correa, Massively parallel first-principles simulation of electron dynamics in materials, J. Parallel Distrib. Comput. **106**, 205 (2017).

[23] N. C. Seeman, DNA in a material world, Nature (London) **421**, 6921 (2003).

[24] See Supplemental Material at http://link.aps.org/supplemental/10.1103/PhysRevLett.130.118401, which includes Refs. [25–47], for computational details, electronic stopping power calculation details and comparisons, charge transfer considerations, and time dependence of DNA hole populations.

[25] W. D. Cornell, P. Cieplak, C. I. Bayly, I. R. Gould, K. M. Merz, D. M. Ferguson, D. C. Spellmeyer, T. Fox, J. W. Caldwell, and P. A. Kollman, A second generation force field for the simulation of proteins, nucleic acids, and organic molecules, J. Am. Chem. Soc. **117**, 5179 (1995); J. Am. Chem. Soc. **118**, 2309(E) (1996).

[26] D. A. Case, T. A. Darden, T. E. Cheatham, C. L. Simmerling, J. Wang, R. E. Duke, R. Luo, M. Crowley, R. C. Walker, and W. Zhang, *Amber 10* (University of California, San Francisco, 2008).

[27] M. J. Abraham, T. Murtola, R. Schulz, S. Páll, J. C. Smith, B. Hess, and E. Lindahl, GROMACS: High performance molecular simulations through multi-level parallelism from laptops to supercomputers, SoftwareX **1–2** (2015).

[28] I. Ivani, P. D. Dans, A. Noy, A. Pérez, I. Faustino, A. Hospital, J. Walther, P. Andrio, R. Goñi, A. Balaceanu, G. Portella, F. Battistini, J. L. Gelpí, C. González, M. Vendruscolo, C. A. Laughton, S. A. Harris, D. A. Case, and M. Orozco, Parmbsc1: A refined force field for DNA simulations, Nat. Methods **13**, 55 (2016).

[29] H. J. C. Berendsen, J. R. Grigera, and T. P. Straatsma, The missing term in effective pair potentials, J. Phys. Chem. **91**, 24 (1987).

[30] B. Hess, H. Bekker, H. J. C. Berendsen, and J. G. E. M. Fraaije, LINCS: A linear constraint solver for molecular simulations, J. Comput. Chem. **18**, 12 (1997).

[31] T. Darden, D. York, and L. Pedersen, Particle mesh Ewald: An N·log(N) method for Ewald sums in large systems, J. Chem. Phys. **98**, 12 (1993).

[32] G. Bussi, D. Donadio, and M. Parrinello, Canonical sampling through velocity rescaling, J. Chem. Phys. **126**, 1 (2007).

[33] F. Gygi, Qbox code, QB@LL version, Lawrence Livermore National Laboratory.

[34] F. Gygi, Architecture of Qbox: A scalable first-principles molecular dynamics code, IBM J. Res. Dev. **52**, 1.2 (2008).

[35] D. R. Hamann, M. Schlüter, and C. Chiang, Norm-Conserving Pseudopotentials, Phys. Rev. Lett. **43**, 1494 (1979).

[36] D. Vanderbilt, Optimally smooth norm-conserving pseudopotentials, Phys. Rev. B **32**, 8412 (1985).

[37] F. Gygi, J.-L. Fattebert, and E. Schwegler, Computation of maximally localized Wannier functions using a simultaneous diagonalization algorithm, Comput. Phys. Commun. **155**, 1 (2003).

[38] A. Castro, M. A. L. Marques, J. A. Alonso, G. F. Bertsch, and A. Rubio, Excited states dynamics in time-dependent density functional theory, Eur. Phys. J. D **28**, 211 (2004).

[39] J. P. Perdew, K. Burke, and M. Ernzerhof, Generalized Gradient Approximation Made Simple, Phys. Rev. Lett. **77**, 3865 (1996).

[40] A. J. Cohen, P. Mori-Sánchez, and W. Yang, Insights into current limitations of density functional theory, Science **321**, 5890 (2008).

[41] J. P. Perdew, M. Ernzerhof, and K. Burke, Rationale for mixing exact exchange with density functional approximations, J. Chem. Phys. **105**, 22 (1996).

[42] K. G. Reeves, Y. Yao, and Y. Kanai, Electronic stopping power in liquid water for protons and alpha-particles from first principles, Phys. Rev. B **94**, 041108 (2016).

[43] D. C. Yost, Y. Yao, and Y. Kanai, Examining real-time time-dependent density functional theory nonequilibrium simulations for the calculation of electronic stopping power, Phys. Rev. B **96**, 115134 (2017).

[44] A. Schleife, Y. Kanai, and A. A. Correa, Accurate atomistic first-principles calculations of electronic stopping, Phys. Rev. B **91**, 014306 (2015).

[45] M. Clayton-Smith and M.-P. Sharma, Renal physiology: Acid–base balance, Anaesth. Intensive Care Med. **22**, 415 (2021).

[46] R. R. Sinden, in *Introduction to the Structure, Properties, and Reactions of DNA, in DNA Structure and Function*, edited by R. R. Sinden (Academic Press, San Diego, 1994), pp. 1–57.

[47] C. Fonseca Guerra, J.-W. Handgraaf, E. J. Baerends, and F. M. Bickelhaupt, Voronoi deformation density (VDD) charges: Assessment of the Mulliken, Bader, Hirshfeld, Weinhold, and VDD methods for charge analysis, J. Comput. Chem. **25**, 2 (2004).

[48] D. C. Yost and Y. Kanai, Electronic excitation dynamics in DNA under proton and α-particle irradiation, J. Am. Chem. Soc. **141**, 13 (2019).

[49] Y. Yao, D. C. Yost, and Y. Kanai, K-Shell Core-Electron Excitations in Electronic Stopping of Protons in Water from First Principles, Phys. Rev. Lett. **123**, 066401 (2019).

[50] Z.-H. Loh *et al.*, Observation of the fastest chemical processes in the radiolysis of water, Science **367**, 6474 (2020).

[51] A. A. Correa, Calculating electronic stopping power in materials from first principles, Comput. Mater. Sci. **150**, 291 (2018).

[52] F. Khan and S. Stathakis, The physics of radiation therapy, Med. Phys. **37**, 1374 (2010).

[53] N. Marzari and D. Vanderbilt, Maximally localized generalized Wannier functions for composite energy bands, Phys. Rev. B **56**, 12847 (1997).

[54] D. C. Yost, Y. Yao, and Y. Kanai, Propagation of maximally localized Wannier functions in real-time TDDFT, J. Chem. Phys. **150**, 19 (2019).

[55] H. H. Rossi and W. Rosenzweig, A device for the measurement of dose as a function of specific ionization, Radiology **64**, 3 (1955).

[56] K. P. Chatzipapas, P. Papadimitroulas, M. Obeidat, K. A. McConnell, N. Kirby, G. Loudos, N. Papanikolaou, and G. C. Kagadis, Quantification of DNA double-strand breaks using Geant4-DNA, Med. Phys. **46**, 405 (2019).

[57] D. Sakata, O. Belov, M. C. Bordage, D. Emfietzoglou, S. Guatelli, T. Inaniwa, V. Ivanchenko, M. Karamitros, I. Kyriakou, N. Lampe, I. Petrovic, A. Ristic-Fira, W. G. Shin, and S. Incerti, Fully integrated Monte Carlo simulation for evaluating radiation induced DNA damage and subsequent repair using Geant4-DNA, Sci. Rep. **10**, 20788 (2020).